Biochemical and Biophysical Research Communications 428 (2012) 160–166

Contents lists available at SciVerse ScienceDirect

Biochemical and Biophysical Research Communications

journal homepage: www.elsevier.com/locate/ybbrc

Vascular insult accompanied by overexpressed heme oxygenase-1 as a pathophysiological mechanism in experimental neurolathyrism with hind-leg paraparesis

Kimino Kawaguchi [a], Fernand Lambein [b], Kuniko Kusama-Eguchi [a,*]

[a] Laboratory of Biochemistry, School of Pharmacy, Nihon University, 7-7-1 Narashinodai, Chiba 274-8555, Japan
[b] Institute Plant Biotechnology for Developing Countries (IPBO), Gent University, K.L. Ledeganckstraat 35, 9000 Ghent, Belgium

ARTICLE INFO

Article history:
Received 4 October 2012
Available online 12 October 2012

Keywords:
Neurolathyrism
Spinal cord
Motor neuron
Hemorrhage
Heme oxygenase-1

ABSTRACT

Neurolathyrism (NL) is a motor neuron disease characterized by spastic paraparesis in the hind legs. β-*N*-oxalyl-L-α,β-diaminopropionic acid (L-β-ODAP), a component amino acid of the grass pea (*Lathyrus sativus* L.), has been proposed as the cause of this disease. In our NL rat model, we previously reported that transient intra-parenchymal hemorrhage occurred in the lower spinal cord during the early treatment period. We show here a possible pathological role of the hemorrhage in motor neuron damage and paraparesis pathology. In the lumbo-sacral spinal cord, blood vessel integrity was lost with numerous TdT-mediated dUTP nick end-labeling-positive blood vessel-like structures occurring simultaneously with the hemorrhage. We observed a coincident >10-fold increase in heme oxygenase-1 (HO-1) only in the lower spinal cord. The early period of paraparesis in the lower leg was greatly suppressed by pretreatment with zinc protoporphyrin IX, a HO-1 inhibitor. *In vitro*, L-β-ODAP was toxic to human umbilical vein endothelial cells compared to L-glutamate. The present data shed light on the role and the mechanism of vascular insult in causing dysfunction and moribund motor neurons in experimental NL.

1. Introduction

Neurolathyrism (NL) is a motor neuron disease characterized by spastic paraparesis in the hind legs. It is due to selective upper and lower motor neuron dysfunction [1,2]. This disorder can be caused by overconsumption over an extended period of time of grass pea (*Lathyrus sativus* L.), which is a drought-tolerant crop. The neuroexcitatory amino acid β-*N*-oxalyl-L-α,β-diaminopropionic acid (L-β-ODAP) is found in grass pea and has been proposed as the cause of the disease [3,4]. Historically, social stress is also considered an important risk factor for NL [5,6]. We reported the development of a NL rat model by repeated parenteral administration of L-β-ODAP, with increased incidence under stress conditions [7]. In each rat with hind-leg paraparesis during the early treatment period, we observed an intraparenchymal hemorrhage in the lumbo-sacral region of the spinal cord that is responsible for hind-leg motor function. It is well known that hemorrhaged blood is highly toxic to neuronal tissues, as is the heme derived from hemoglobin (Hb). However, whether this hemorrhage plays a role in motor neuron death as a pathogenic mechanism in NL remains unclear.

Recent studies have demonstrated that impairment of the blood–spinal cord barrier is an additional phenomenon in an amyotrophic lateral sclerosis mice model [8,9] and results in microhemorrhages with the release of neurotoxic Hb-derived products, reductions in microcirculation, or hypoperfusion [10]. In response to a vascular insult, signals from neurons and astrocytes recruit microglia, which secrete several proinflammatory cytokines when activated [11], further aggravating neuronal injury and synaptic dysfunction. As NL is also a motor neuron disease, it is reasonable to expect that changes in the vasculature will make an important contribution to motor neuron damage.

In this study, we focused on heme oxygenases (HO), the rate-limiting enzymes in heme degradation. There are two active HO isoenzymes: inducible HO-1 and constitutively active HO-2. HO-1 is induced by many stimuli including heme, various stresses, hemorrhage and hypoxia via nuclear erythroid-derived 2-related factor 2 cascade [12]. HO-1 has cytoprotective properties mediated by heme degradation products such as carbon monoxide (CO), ferrous iron, and biliverdin, which is converted to bilirubin by oxidation. On the other hand, excessive HO-1 can become toxic in some conditions [13].

The aim of the present work was to investigate the pathological changes in the early period of paraparesis. We investigated histopathological changes in the lumbar motor neurons and in the sur-

* Corresponding author. Fax: +81 47 4655340.
E-mail address: kusama.kuniko@nihon-u.ac.jp (K. Kusama-Eguchi).

0006-291X/$ - see front matter © 2012 Elsevier Inc. All rights reserved.
http://dx.doi.org/10.1016/j.bbrc.2012.10.032

rounding blood vessels, and attempted to clarify whether HO-1 plays a role in the NL model rat.

2. Materials and methods

2.1. Animals

Animal experiments were performed according to the guidelines of the College of Pharmacy, Nihon University. The experimental protocol was submitted to and approved by the ethics committee for animal experimentation of the College of Pharmacy, Nihon University. Wistar/ST specific pathogen-free rats were purchased from Japan SLC (Shizuoka, Japan). Rats were bred domestically and kept at 23 ± 1 °C at a relative humidity of 50 ± 10% and maintained under a 12-h light–dark cycle (lights on between 8:00 and 20:00).

2.2. Neurolathyrism models

Rat treatment with L-β-ODAP (Lathyrus Technologies, Hyderabad, India) was performed as described previously [14].

2.3. Effect of zinc protoporphyrin IX (ZnPP) in NL model rats

Postnatal day 1 rats ($n = 86$) were separated into four groups. Group 1 ($n = 28$) was subcutaneously (sc) treated with L-β-ODAP and intraperitoneally (ip) treated with 50% (v/v) dimethyl sulfoxide (DMSO); the latter was given 1 h before L-β-ODAP. Group 2 ($n = 16$) was treated with saline and 50% DMSO, the latter treated 1 h before. Group 3 ($n = 27$) was treated with L-β-ODAP and ZnPP dissolved in 50% DMSO, ip; the latter was given 1 h before the L-β-ODAP. Group 4 ($n = 15$) was treated with 50 mg/kg ZnPP and 1 h later treated with saline.

2.4. Histochemistry

Rat spinal cords were fixed by immersing the isolated sample in 4% paraformaldehyde (PFA) for 24 h. Tissue was cryoprotected in serial phosphate–buffered sucrose solutions (10%, 20%, and 30%) at 4 °C, and then the L3–L4 spinal cords were cut into 10-μm thick sections with a cryostat. The sections were post-fixed in 4% PFA and then permeabilised with 0.1% Triton X-100/PBS. Endogenous peroxidase activity was blocked with 0.3% H_2O_2/methanol for 30 min. Sections were autoclaved at 120 °C for 10 min in 10 mM sodium citrate buffer (pH 6.0) for antigen retrieval, and blocked in 5% horse serum/PBS. Sections were incubated with anti-vascular endothelial growth factor receptor-1 (1:200, Santa Cruz Biotechnology, CA, USA) or anti-HO-1 (1:400, Enzo Life Science, Farmingdale, NY, USA) overnight at 4 °C, and detected with the Vectastain Elite ABC kit (Vector Laboratories, Burlingame, CA, USA) following manufacturer's instructions followed by development with the 3,3-diaminobenzidine Peroxidase Substrate kit (Vector Laboratories). Sections were lightly counterstained with hematoxylin, dehydrated and mounted. To confirm the specificity of the primary antibody, a sample set was stained in a similar manner but without the primary antibodies. Sections were acquired using an Olympus IX-70 (Olympus, Japan) inverted microscope equipped with the DP70 CCD camera. Imaging data were processed in Photoshop (CS3; Adobe Systems, San Jose, CA) using proportional adjustments and/or color balancing.

2.5. Immunofluorescence

Cryostat sections were fixed in cold acetone for 5 min, permeabilised with 0.1% TritonX-100/PBS, and blocked in 1% BSA/PBS for 1 h at room temperature. Sections were incubated with SMI-32 antibodies (a mouse monoclonal antibody against non-phosphorylated neurofilament H, 1:1000, Covance, Berkeley, CA, USA) overnight at 4 °C. The primary antibodies were visualized using AlexaFluor 488 anti-mouse secondary antibody (1:2500, Invitrogen, Carlsbad, CA, USA). Sections were analyzed using a confocal laser-scanning microscope LSM510 (Carl Zeiss, Jena, Germany).

2.6. TdT-mediated dUTP nick end-labeling (TUNEL) staining

TUNEL was performed using a TACS2 TdT Blue Label Kit (Trevigen, Gaithersburg, MD, USA) according to the manufacturer's instructions.

2.7. Quantitative real-time reverse-transcriptase polymerase chain reaction (RT-PCR) analysis

Total RNA from the spinal cord was extracted using QIAzol Lysis Reagent (Qiagen, Hilden, Germany) and purified with an RNeasy Lipid tissue Mini kit (Qiagen) according to the manufacturer's instructions. mRNA quantification was performed using a two-step real-time RT-PCR on a DNA Engine Thermal Cycler (Bio-Rad, Hercules, CA, USA) according to the manufacturer's instructions. The quantitative PCR reaction was performed using a SYBR Premix Ex Taq Kit (Takara, Japan) on a Mx3000P QPCR machine (Agilent Technologies, Spain). Cycling conditions for all target genes were as follows: 95 °C for 5 min, 40 cycles of 95 °C, 30 s; 60 °C, 30 s; 75 °C, 20 s. β-Actin was amplified as a housekeeping gene. The sequences of the HO-1 primers were based on nucleotides 718–979 of rat HO-1 mRNA [15]. 5′-AAGAGGCTAAGACCGCCTTC-3′ (forward); 5′-GCATAAATTCCCACTGCCAC-3′ (reverse).

β-Actin; GenBank association No. NM_031144; 5′-AGCCATGTACGTAGCCATCC-3′ (forward); 5′-CTCTCAGCTGTGGTGGTGAA-3′ (reverse).

2.8. Cell culture

Human umbilical vein endothelial cells (HUVECs) were purchased from Cell Applications (San Diego, CA, USA). Cells were grown in EGM-2 BulletKit (Lonza, Allendale, NJ, USA) at 37 °C in a humidified atmosphere of 5% CO_2 and 95% air.

2.9. Cytotoxicity assay

HUVECs (2×10^4 cells/well) were seeded into 96-well plates. After 24 h incubation with various drug concentrations in Endothelial Based Medium-2 (Lonza), the culture supernatants were collected. The lactate dehydrogenase assay was performed using the Lactate Dehydrogenase Activity Assay kit (Cayman Chemical, Ann Arbor, MI) according to the manufacturer's instructions.

2.10. Western blot

Primary antibodies; anti-mouse HO-1 (1:1000) and anti-rabbit HO-2 (1:1000) were purchased from Enzo Lifescience and anti-mouse beta-tubulin (1:2000) was purchased from Promega (Madison, WI, USA). Horseradish peroxidase-conjugated anti-rabbit or mouse IgG secondary antibodies (1:5000) were purchased from Santa Cruz. Details of Western blot have been published elsewhere [7].

2.11. Statistical analysis

All data are expressed as the mean ± SEM. Statistical analyses were performed using one-way analysis of variance (ANOVA) followed by Tukey–Kramer multiple comparison test. Statistical significance was set at $p < 0.05$.

3. Results

3.1. Disruption of blood vessels and injury to the lumbar spinal motor neurons in hind-leg paraparetic rats

We previously reported that repeated parenteral injection of L-β-ODAP resulted in hind-leg paraparetic rats, and that these NL model rats always showed transient intraparenchymal hemorrhage in the lower spinal cord during the early period of hind-leg paraparesis [7]. A longitudinal section of the lower spinal cord showed that the hemorrhage was scattered within each segment and occurred mainly in the ventral horn of the lumbar spinal cord, and in both ventral and dorsal sides of the sacral region (Fig. 1B). Transverse sections also showed that the hemorrhage occurred mainly in the ventral horn of the lumbar spinal cord (Fig. 1F). To elucidate the earliest pathological events in this model, we investigated histopathological changes in blood vessels and motor neurons of the lower spinal cord where topical hemorrhage occurred. Hematoxylin and eosin staining of longitudinal sections of control rat lumber spinal cord showed healthy vascular structures (Fig. 1C; arrowhead), whereas they could hardly be seen in the paraparetic rat (Fig. 1E). We also immunostained the lumbar spinal cords of control and paraparetic postnatal day 2 (P2) rats with vascular endothelial growth factor receptor-1 (VEGFR-1) antibody as an endothelial marker. Compared to numerous thread-like staining in the control slice (Fig. 1G, arrowheads), the lumbar spinal cord of paraparetic rats showed fewer integrated structures that were positive for VEGFR-1 except enhanced staining with nuclei (Fig. 1H). These results indicated that the integrity of vascular structures was lost during the early period of paraparesis with concomitant hemorrhage. Immunofluorescence staining was greatly decreased for SMI-32, a motor neuron marker, at the site of the hemorrhage (Fig. 1J). These results suggested that hemorrhage in and around lamina IX in the lower region resulted in substantial damage to motor neurons, consistent with motor dysfunction in the lower extremities.

3.2. The emergence of TUNEL-positive blood vessel-like structures in the lumbar spinal cord of paraparetic rats

To examine whether there were damages in the blood vessels in the paraparetic rats, we performed the TUNEL assay in P2 rats. TUNEL-positive apoptotic cells are shown in dark blue against pink counter-staining. Significant increases in thin, TUNEL-positive

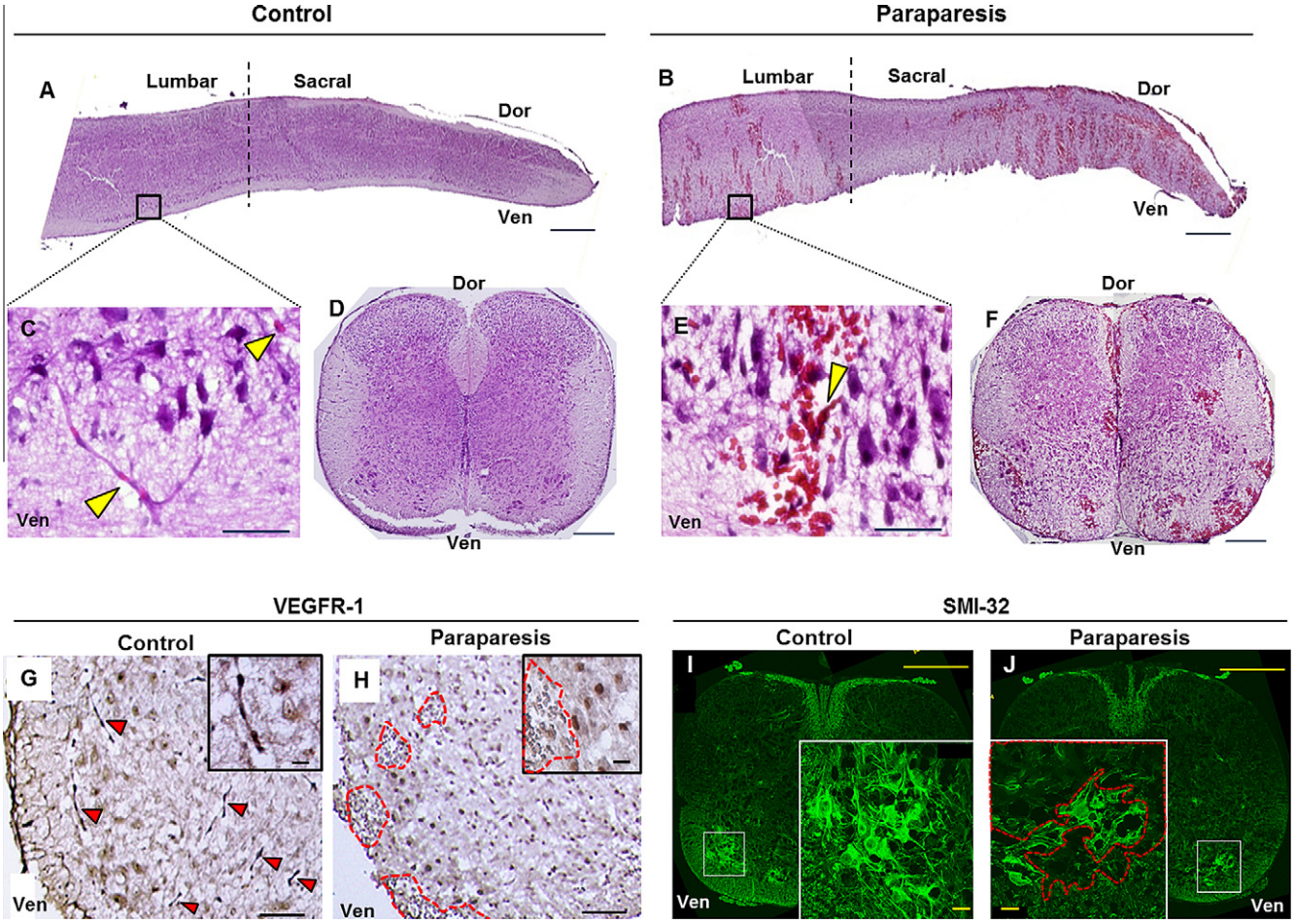

Fig. 1. Pathological features of the model rat lumbar spinal cord showing hemorrhage, motor neuron damage and vascular insult. (A and B) Longitudinal sections of the lower spinal cord of control and paraparetic postnatal day 2 (P2) rats. Scale bars = 500 μm. (C and E) Enlarged view of (A) and (B), respectively. The yellow arrowheads show blood vessels. Scale bars = 50 μm. (D and F) Transverse sections of the lumbar spinal cord of control and paraparetic P2 rats. Scale bars = 200 μm. Sections in (A–F) were stained with hematoxylin and eosin. Hemorrhage; scarlet color. (G and H) Transverse sections of immunostained with VEGFR-1 in control and paraparetic rats at P2. Scale bar = 100 μm. The inset of (G and(H) are enlarged images. Scale bars = 20 μm. The red arrowheads show blood vessels (G). (I and J) Transverse sections were immunostained with SMI-32 antibody in the lumbar spinal cord of control and paraparetic P2 rats. Scale bars = 200 μm. The inset of (G and J) are enlarged images. Scale bars = 20 μm. Dotted red circles show the hemorrhage (H and J). Dos, dorsal; Ven, ventral.

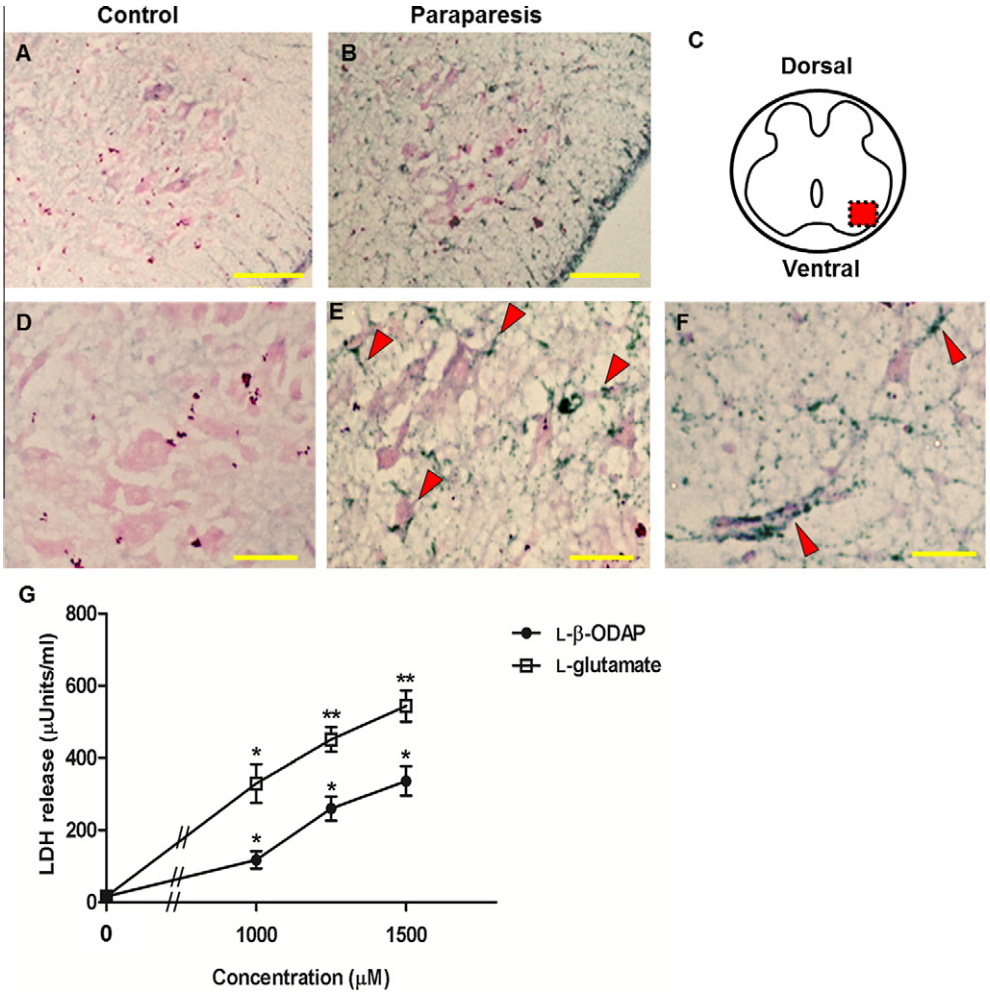

Fig. 2. Apoptosis of blood vessel-like structures in the lumbar spinal cord of paraparetic rats (upper) and *in vitro* damage of human umbilical vein endothelial cells (HUVECs) caused by L-β-ODAP. (A and B) TdT-mediated dUTP nick end-labeling (TUNEL) staining of the lumbar ventral horn of control or paraparetic postnatal day 2 rats. Ven = ventral. Scale bar = 200 μm. (C) Diagram of the spinal cord; red square shows area of Fig. (D–F). (D) A higher magnification view of control lumbar cord. (E and F) A higher magnification view of paraparesis lumbar cord. Scale bar = 50 μm. The arrowheads show TUNEL-positive apoptotic cells (dark blue). Pink: counterstaining with nuclear fast red. (G) L-β-ODAP and L-glutamate had a concentration-dependent toxic effect on HUVECs. Values are units of LDH released into medium and the means ± SEM. $n = 3$. Significantly different LDH release compared to no L-β-ODAP or L-glutamate ($^{*}p < 0.05$, $^{**}p < 0.01$).

blood vessels and/or peripheral structures were observed in the lumbar spinal cord of paraparetic rats (Fig. 3E and F). Most motor neurons did not show apoptotic cell death in this period. Therefore, apoptosis in blood vessels in the lumbar spinal cord of paraparetic rats occurred mainly during the earlier period, before motor neurons underwent apoptosis [7].

3.3. L-β-ODAP had a direct toxic effect on HUVECs

Histological examination of the lumbar spinal cord samples of NL model rats revealed disruption of blood vessels. To determine whether L-β-ODAP had any direct toxic effect on vascular endothelial cells, we measured the cytotoxicity on HUVECs using the lactate dehydrogenase (LDH) method. We found a direct toxic effect of L-β-ODAP on HUVECs in a concentration-dependent manner (Fig. 2G). L-glutamate-induced cytotoxicity (Fig. 2G) and thapsigargin-induced endoplasmic reticulum stress (LDH release; 131 ± 32 μUnit/ml at 0.5 nM and 240 ± 32 μUnit/ml at 20 nM) were used as controls. These reagents also had a toxic effect on HUVECs in a concentration-dependent manner.

3.4. Heme oxygenase (HO)-1 expression were greatly increased in the lower spinal cord of paraparetic rats

To further attempt to understand the link between motor neuron damage and the disruption of blood vessels, we focused on HO-1, which is induced by heme or hemorrhage-induced hypoxia. We examined the expression level of HO-1 mRNA in the spinal cord of paraparetic and control P2 rats using real-time RT-PCR. HO-1 mRNA was significantly increased by as much as 10-fold in the lower spinal cord of paraparetic rats compared with control rats (Fig. 3A). We next examined HO-1 protein expression using Western blot analysis. More than a 12-fold increase in HO-1 protein was observed only in the lower spinal cord, similar to the increase in mRNA expression (Fig. 4B and C). On the other hand, protein expression of the constitutively active enzyme HO-2 was not changed (Fig. 4B and D).

3.5. The onset of hind-leg paraparesis was suppressed by the HO-1 inhibitor, ZnPP

We investigated whether HO-1 induction affected the incidence of hind-leg paraparetic pups. Postnatal day 1 rats were pretreated

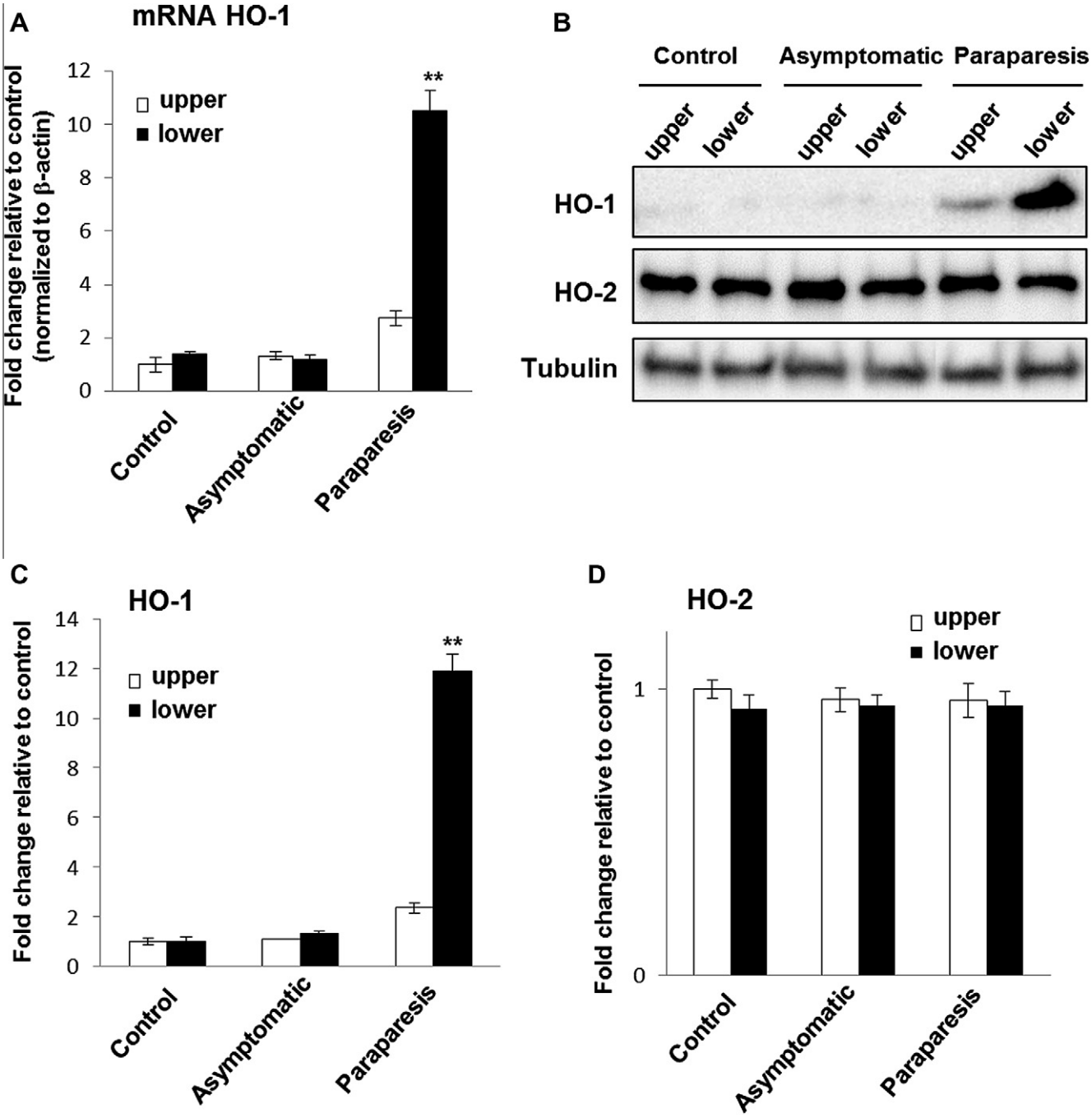

Fig. 3. Heme oxygenase-1 (HO-1) expression was increased in the lower spinal cord of paraparetic rats. Spinal cords of postnatal day 2 (P2) rats were dissected into upper (cervical and thoracic) and lower (lumbar and sacral) region by cutting them at the 13th rib level. (A) Quantitative RT-PCR analysis of mRNA transcripts for HO-1 in the upper or lower spinal cords from control, asymptomatic, and paraparetic P2 rats. mRNA expression was normalized to that of β-actin, and fold change is expressed relative to control rats (means ± SEM. $n = 4$ rats per group. $^{**}p < 0.01$). (B) Immunoblotting for HO-1 (top), HO-2 (middle), and tubulin (bottom) protein in the upper or lower spinal cords from control, asymptomatic, and paraparetic P2 rats (means ± SEM. $n = 4$ rats per group). (C and D) Band density for test proteins relative to tubulin ($^{**}p < 0.01$).

intraperitoneally with 50 mg/kg ZnPP, a HO-1 inhibitor, 1 h before L-β-ODAP administration. The effect of combined treatment of L-β-ODAP and ZnPP greatly suppressed the incidence of paraparesis to 1.9 ± 1.9% compared to the L-β-ODAP group (42.4 ± 1.3%) in P2 rats (Fig. 4A). Toxic effects of ZnPP alone and DMSO, which was used as a diluent of ZnPP, were not seen. Next we investigated the *in situ* expression of HO-1 in the lumbar spinal cord. We immunostained lumbar spinal cord sections of P2 rats with the HO-1 antibody. Increased HO-1 staining in the lumbar spinal cord of paraparetic rats of L-β-ODAP and DMSO administrated group were seen (Fig. 4C), whereas HO-1 expression levels were relatively low in the lumbar spinal cord of control rat; saline and DMSO administrated rats and saline and ZnPP administrated rats (Fig. 4B and D). These data are consistent with the Western blot results. Furthermore, HO-1 staining decreased in the lumbar spinal cord of L-β-ODAP and ZnPP administrated rats which do not show signs of paraparesis (Fig. 4E). These data strongly indicate that induction of HO-1 is involved in the development of paraparesis in NL rat models. HO-1 was expressed in the lumbar spinal motor neurons of paraparetic rats (Fig. 4C arrows).

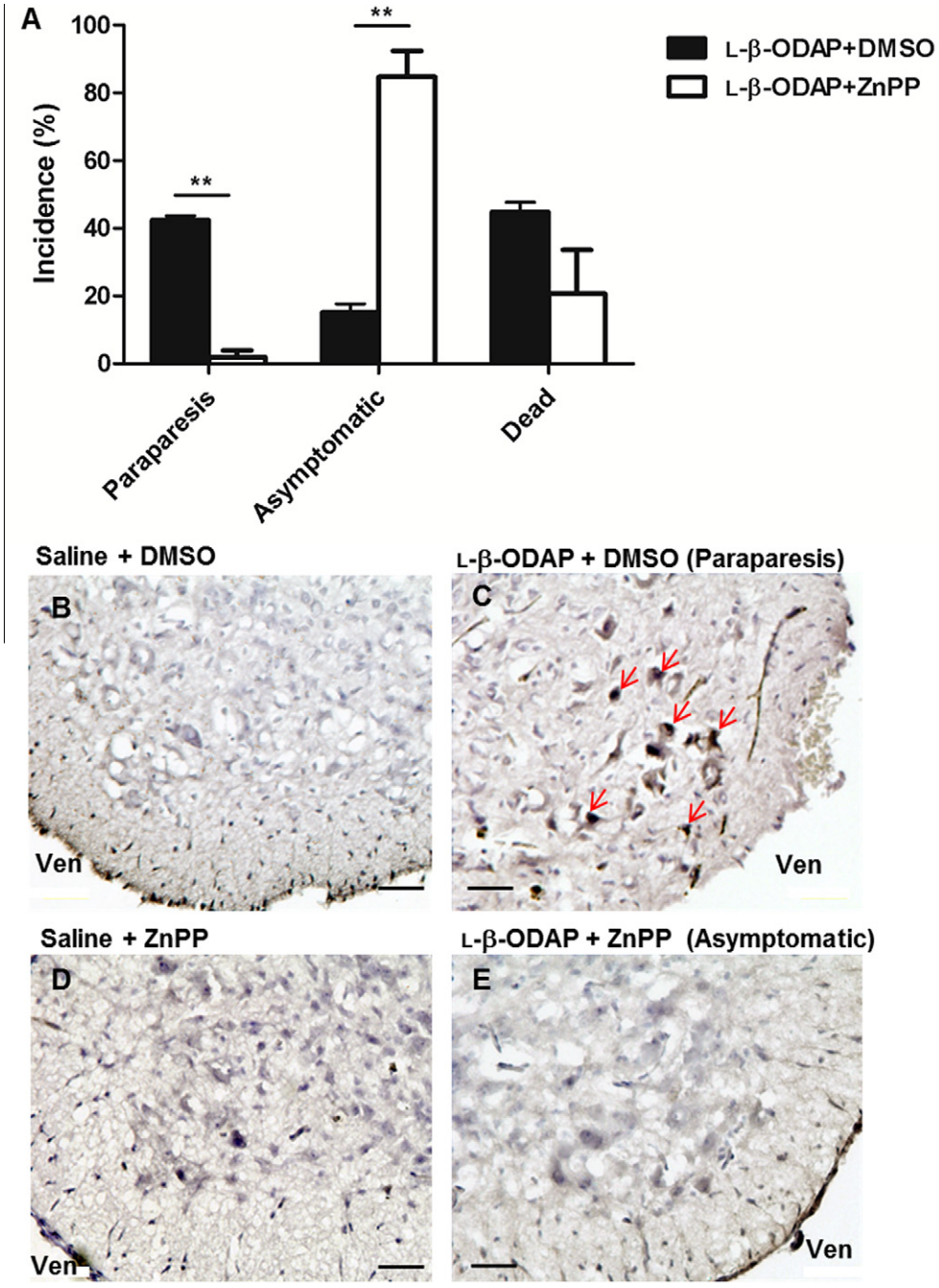

Fig. 4. Suppression of hind-leg paraparesis incidence by pretreatment with zinc protoporphyrin IX (ZnPP). (A) Three independent sets of experiments with a total of 86 rat pups of both sexes were used. Treatments were as described in Materials and methods. Data were expressed as percent incidence calculated with the following equations (*n* means number of animals): L-β-ODAP and DMSO administrated group Paraparesis = 1 − {1 − (*n* of paraparesis in gruop1/total *n* in group 1)/(*n* of paraparesis of in group 2/total *n* in group 2)} × 100, for other data, replace the term in the above equation paraparesis with asymptomatic or dead, respectively. L-β-ODAP and ZnPP administrated group Paraparesis = 1 − {1 − (*n* of paraparesis in group 3/total *n* in group 3)/(*n* of paraparesis in group 4/total *n* in group 4)} × 100, for other data, replace the term in the equation paraparesis with asymptomatic or dead, respectively. The term "asymptomatic" means those that showed no sign of paraparesis. No rats were paraparetic nor dead in groups 2 and 4. (B–E) Immunohistochemical staining for HO-1 in the ventral horn of the lumbar spinal cord of L-β-ODAP + DMSO administrated group, which showed sign of paraparesis (B), Saline + DMSO administrated group (C), L-β-ODAP + ZnPP administrated group, which showed no sign of paraparesis (D) and Saline + ZnPP administrated group (E). Arrowheads; HO-1 positive-cells. Ven; ventral. Scale bar = 50 μm.

4. Discussion

Neurons and the vasculature not only are anatomically closely tied to each other, but they also respond to common signals to the wiring of their networks [16]. Using our rat model of NL, we found that blood vessel was unusual in the lumbar spinal cord (Fig. 1). As shown in our previous report, the tissue content of L-β-ODAP was highest in the lower half compared to the upper half of the spinal cord, and was scarcely found in the brain of L-β-ODAP-treated rat pups [14]. This distribution may reflect the leaky features of the blood vessels of the lower spinal cord, resulting in the higher tissue content of the toxin. Our *in vitro* data showing

that L-β-ODAP is toxic to HUVECs (Fig. 2) are important and suggest that one of the primary targets of L-β-ODAP is the endothelial cell *per se*, and the early disruption of a physical barrier, i.e., the endothelium and/or some resultant changes in signals including VEGF receptors may have caused the hemorrhage [7]. We previously reported the occurrence of apoptotic/necrotic motor neurons, which peaked around days 4 and 5 [7].

Our current findings show that some important events in the blood vessel and surrounding structures preceded motor neuron death. Similar insults in vasculature were recently reported in human amyotrophic lateral sclerosis cases [17]. Therefore, we consider that a defect in the cross-talk between neurons and vascular cells may result in neuronal damage in experimental NL. In addition, we also observed increased tumor necrosis factor-α (TNF-α) and inteleukin-6 expression (data not shown), which will also have a deteriorating effect both on blood vessels and neurons.

We observed symptom-specific overexpression of the novel key factor, HO-1, in NL pathogenesis in the lumbo-sacral spinal cord by as much as 10-fold. HO-1 expression is induced by hemolysis, or hemosiderin, the latter of which we also observed in this study (data not shown). In addition, TNF-α has been reported to induce HO-1 in endothelial cells [18]. As we also observed a 4.5-fold, stimultaneous increase in the TNF-α mRNA, the HO-1 induction would also have been enhanced.

Two questions remain: what cell type is most influenced in this situation to induce higher HO-1 expression, and what pathway following HO-1 induction is related to vascular insult; we hypothesized that this unidentified pathway plays role in motor neuron dysfunction. In the central nervous system, insults such as contusion or microbe infection of any major constituent of cells in the parenchyma can induce HO-1. Astrocyte HO-1 has been shown to be neuroprotective [19], whereas HO-1 knockout in microglia ameliorates brain hemorrhage [20]. The roles of HO-1 in two brain regions, the cerebral cortex and hippocampus, were reported to be different [21]. These data show that cell-specific HO-1 expression and its regulation are key factors in neuronal damage and in certain types of neurodegeneration. The unusually high level of HO-1, as much as 10-fold by itself or its products Fe^{2+} and/or CO, may be damaging to motor neurons. In Parkinsonism and Alzheimer's disease, a pathogenic role for reactive oxygen species from the Fenton reaction and accumulated Fe^{2+} in the brain has been reported [22]. Motor neuron damage and accompanying motor dysfunction could be caused by these products.

We observed a dramatic reduction in the incidence of paraparesis with pretreatment with ZnPP (Fig. 4). Interestingly, in the ZnPP and L-β-ODAP administered group, a few rats were observed with hemorrhage in the lower spinal cord but with no sign of hind-leg paraparesis. A possible explanation is that even if endothelial cells were injured by L-β-ODAP and hemorrhage followed, ZnPP inhibited HO-1 and/or its toxic action, thus rescuing motor neurons from becoming dysfunctional.

In summary, blood vessel disruption and hemorrhaged blood itself showed profound insults on motor neurons of the lower spinal cord in NL model rats. Overexpressed HO-1 was the cause of motor neuron death by itself and was probably due to its enzymatic products present in our model and possibly in other motor neuron dysfunction. A novel therapy targeting excess HO-1 may be worth exploring for use in motor neuron diseases and spinal cord injury.

Acknowledgments

We are grateful to Mr. Shin-ichi Yamada, B.S. and Ms. Naoko Harayama, B.S. for their technical assistance. This work was supported by a Grant-in-Aid for Scientific Research (C) #2259088 2010-12 from the Japan Society for the Promotion of Science, and by a Nihon University Multidisciplinary Research Grant for 2012.

References

[1] A.C. Ludolph, P.S. Spencer, Toxic models of upper motor neuron disease, J. Neurol. Sci. 139 (1996) 53–59.
[2] D.D. Tshala-Katumbay, P.S. Spencer, Toxic disorders of the upper motor neuron system, in: A.A. Eisen, P.J. Shaw (Eds.), Handbook of Clinical Neurology 82, Motor Neuron Disorders and Related Diseases, Elsevier, B.V., 2007, pp. 353–372.
[3] H. Getahun, A. Mekonnen, R. TekleHaimanot, F. Lambein, Epidemic of neurolathyrism in Ethiopia, Lancet 354 (1999) 306–307.
[4] F. Lambein, Y.H. Kuo, K. Kusama-Eguchi and F. Ikegami, 3-N-oxalyl-L-2,3-diaminopropanoic acid, a multifunctional plant metabolite of toxic reputation, ARKIVOC (ix), 2007, 45–52.
[5] P.S. Spencer, Lathyrism, In: B.G. Vinken (Ed.), Handbook of Clinical Neurology, Intoxication of the Nervous System, Part II, vol. 65. Elsevier, North Holland, 1995, pp. 1–20.
[6] K. Kawaguchi, S. Yamada, K. Kusama-Eguchi, CCDN News 19 (2012) 2–3.
[7] K. Kusama-Eguchi, Y. Yamazaki, T. Ueda, A. Suda, Y. Hirayama, F. Ikegami, K. Watanabe, M. May, F. Lambein, T. Kusama, Hind-limb paraparesis in a rat model for neurolathyrism associated with apoptosis and an impaired vascular endothelial growth factor system in the spinal cord, J. Comp. Neurol. 518 (2010) 928–942.
[8] S. Garbuzova-Davis, S. Saporta, E. Haller, I. Kolomey, S.P. Bennett, H. Potter, P.R. Sanberg, Evidence of compromised blood–spinal cord barrier in early and late symptomatic SOD1 mice modeling ALS, PLoS One 2 (2007) e1205.
[9] C. Nicaise, D. Mitrecic, P. Demetter, R. De Decker, M. Authelet, A. Boom, R. Pochet, Impaired blood–brain and blood–spinal cord barriers in mutant SOD1-linked ALS rat, Brain Res 1301 (2009) 152–162.
[10] Z. Zhong, R. Deane, Z. Ali, M. Parisi, Y. Shapovalov, M.K. O'Banion, K. Stojanovic, A. Sagare, S. Boillee, D.W. Cleveland, B.V. Zlokovic, ALS-causing SOD1 mutants generate vascular changes prior to motor neuron degeneration, Nat. Neurosci. 11 (2008) 420–422.
[11] S. Man, E.E. Ubogu, R.M. Ransohoff, Inflammatory cell migration into the central nervous system: a few new twists on an old tale, Brain. Pathol. 17 (2007) 243–250.
[12] J. Alam, J.L. Cook, Transcriptional regulation of the heme oxygenase-1 gene via the stress response element pathway, Curr. Pharm. Des. 19 (2003) 2449–2511.
[13] D.M. Suttner, P.A. Dennery, Reversal of HO-1 related cytoprotection with increased expression is due to reactive iron, FASEB J. 13 (1999) 1800–1809.
[14] K. Kusama-Eguchi, F. Ikegami, T. Kusama, A. Suda, Y. Ogawa, K. Igarashi, K. Watanabe, A rat model of neurolathyrism: repeated injection of L-beta-ODAP induces the paraparesis of the hind legs, Amino Acids 28 (2005) 139–143.
[15] S. Shibahara, R. Müller, H. Taguchi, T. Yoshida, Cloning and expression of cDNA for rat heme oxygenase, Proc. Natl. Acad. Sci. USA 82 (1985) 7865–7869.
[16] P. Carmeliet, M. Tessier-Lavigne, Common mechanisms of nerve and blood vessel wiring, Nature 436 (2005) 193–200.
[17] S. Garbuzova-Davis, D.G. Hernandez-Ontiveros, M.C. Rodrigues, E. Haller, A. Frisina-Deyo, S. Mirtyl, S. Sallot, S. Saporta, C.V. Borlongan, P.R. Sanberg, Impaired blood–brain/spinal cord barrier in ALS patients, Brain Res. 1469 (2012) 114–128.
[18] C.M. Terry, J.A. Clikeman, J.R. Hoidal, K.S. Callahan, TNF-alpha and IL-1alpha induce heme oxygenase-1 via protein kinase C Ca2+ and phospholipase A2 in endothelial cells, Am. J. Physiol. 276 (1999) H1493–H1501.
[19] M.R. Vargas, M. Pehar, P. Cassina, L. Martínez-Palma, J.A. Thompson, J.S. Beckman, L. Barbeito, Fibroblast growth factor-1 induces heme oxygenase-1 via nuclear factor erythroid 2-related factor 2 (Nrf2) in spinal cord astrocytes, J. Biol. Chem. 280 (2005) 25571–25579.
[20] J. Wang, S. Doré, Heme oxygenase-1 exacerbates early brain injury after intracerebral haemorrhage, Brain 130 (2007) 1643–1652.
[21] M. Ohnishi, H. Katsuki, K. Unemura, Y. Izumi, T. Kume, Y. Takada-Takatori, A. Akaike, Heme oxygenase-1 contributes to pathology associated with thrombin-induced striatal and cortical injury in organotypic slice culture, Brain Res. 1347 (2010) 170–178.
[22] B. Uttara, A.V. Singh, P. Zamboni, R.T. Mahajan, Oxidative stress and neurodegenerative diseases a review of upstream and downstream antioxidant therapeutic options, Curr. Neuropharmacol. 7 (2009) 65–74.